symmetry

MDPI

Article

A Highly Efficient Infinity-Shaped Large Angular- and Polarization-Independent Metamaterial Absorber

Meshari Alsharari [1,*], Bo Bo Han [2], Shobhit K. Patel [3], Jaymit Surve [4], Khaled Aliqab [1] and Ammar Armghan [1,*]

[1] Department of Electrical Engineering, College of Engineering, Jouf University, Sakaka 72388, Saudi Arabia
[2] Department of Information and Communication Technology, Marwadi University, Rajkot 360003, Gujarat, India
[3] Department of Computer Engineering, Marwadi University, Rajkot 360003, Gujarat, India
[4] Department of Electrical Engineering, Marwadi University, Rajkot 360003, Gujarat, India
* Correspondence: mmaalsharari@ju.edu.sa (M.A.); aarmghan@ju.edu.sa (A.A.)

Abstract: An efficient diagonally symmetric infinity-shaped broadband solar absorber has been demonstrated in this research paper. The structure was developed with an infinity-shaped resonator made of titanium (Ti) and gallium arsenide (GaAs) at the base substrate layer to achieve absorption in a wideband spectrum under solar energy radiation, and absorption efficiencies were calculated employing the finite element method. The average solar energy absorption spectrum ranges from the ultraviolet to the mid-infrared regions, and 93.93% average absorption in this band is achieved. Moreover, bandwidths of 2800 and 1110 nm were observed, and, in these bands, we attained continuous absorption above 90% and 95%, respectively, with average absorption rates of 93.93% and 96.25%, respectively. Furthermore, based on this solar energy absorber, which was optimized after varying many design parameters, it is also observed that the developed design is angle-insensitive from 0° to 50° and polarization-insensitive from the results of the transverse electric (TE) and transverse magnetic (TM) modes. The developed infinity-shaped broadband solar absorber design is highly efficient and provides broadband absorptance that can be used as an absorber layer in solar cells.

Keywords: metamaterial absorber; broadband absorption; refractory material; large angular; polarization-independent

check for updates

Citation: Alsharari, M.; Han, B.B.; Patel, S.K.; Surve, J.; Aliqab, K.; Armghan, A. A Highly Efficient Infinity-Shaped Large Angular- and Polarization-Independent Metamaterial Absorber. *Symmetry* **2023**, *15*, 352. https://doi.org/10.3390/sym15020352

Academic Editors: Ben-Xin Wang, Han Xiong and Qi Lin

Received: 23 December 2022
Revised: 11 January 2023
Accepted: 16 January 2023
Published: 28 January 2023

1. Introduction

By the invention of new techniques that use natural resources [1], we can reduce the damage to our environment and improve the sustainability of Earth. Among the many developed technologies, solar power technique is the generation of electricity from the sun, and it is one of the effective ways to solve the global warming problem that we are facing now. Electricity generation using solar energy is an efficient and cost-effective medium that is much better than using fossil fuels [2]. Moreover, the production of electricity by fossil fuels can cause accidents during the generation and transportation of fossil fuels [3]. On the other hand, solar energy generates electricity through chemical reactions that radiate directly from the sun [4]. Therefore, the sun, a very potent energy source that will not run out anytime soon, can be employed for the major generation of efficient and clean energy [5].

A solar cell is a type of electronic device that uses the photovoltaic effect to directly convert light energy into electrical energy [6]. The type of solar energy that the cell can transform into electricity is referred to as solar cell efficiency. If a solar panel is 20 percent efficient, it can produce electricity from 20 percent of the sunlight that strikes it [7]. The temperature has an impact on the solar cell's maximum power point. There are numerous techniques to raise solar cells' effectiveness [8]. Increasing the semiconductor's purity, employing more effective semiconducting materials, such as gallium arsenide, adding more layers or p-n junctions to the cell, and concentrating solar energy using concentrated photovoltaics are a few of these techniques. Solar cells and solar absorbers are not the same thing; solar absorbers do not produce electricity from solar energy [9–11]. They transform solar energy into heat and are an integral part of solar cells, and the higher amount of solar energy they absorb means that electricity generation can be increased. Metamaterials do not exist in nature; they are artificially-engineered materials [12]. For broadband absorber design enhancement, we need to make some improvements, such as selecting the appropriate material, size, etc. Broadband absorber nanostructure design is still an ongoing research topic [13].

A typical absorber is a metal–dielectric–metal structure with three layers [14]. In the initial stage, this kind of absorber achieves the narrow band (single band, dual band, multi-band) [15] absorption response that is suitable for various sensing [16] and encoding [17] applications. The fabrication of metamaterial absorbers has employed techniques such as two-layer, three-layer, four-layer, and multi-layer to achieve maximum absorption in the optical region, but three-layered structures have been the most popular [18]. The bottom plane and resonator's coupling capacitance is formed by the three-layer (metal–dielectric–metal) construction [19]. The semiconducting substance known as the absorber layer is frequently referred to as the heart of all thin-film solar cells. The second layer in the solar absorber is the substrate layer, and it has a high absorption rate [20]. The ground layer stops the waves from transmitting because the ground layer is built of metal [21]. Broadband and extremely effective optical absorption, with little transmittance and reflection over the full solar spectrum, occurs in a perfect solar absorber between 300 and 2500 nm, as per Liu and his co-authors. Zheng and his investigators observed that the average absorption rate in the range of 288.5 to 2157.5 nm is 96.56%, and the average absorption efficiency for the entire band (200–2600 nm) is 93.77% [22]. According to Qin's theory, a broadband absorber's primary solar radiation zone has an absorption rate of more than 93% [23]. Wu et al. reported the results with an average absorption of 98% for regular incident lights over the spectral range of 380 to 2000 nm. Broadband absorption in the spectrum region of 378 to 626 nm has been proposed to be achieved using a gold nanotriangle array backed with a metallic mirror. A device that displays above 90% absorption, from 354 to 1066 nm, is made of a silica cube array sandwiched between a titanium cube array and a continuous aluminum mirror [24]. Zhou and his co-authors demonstrated that the metamaterial solar absorber can attain an average absorption rate of 97.6% between 400 and 2500 nm [25].

In this paper, two types of material, including gallium arsenide (GaAs) and titanium (Ti), have been used. One of the crucial semiconductor materials with high efficiency is gallium arsenide (GaAs) [26]. GaAs (gallium arsenide) is most commonly used in solar cells because it absorbs more energy due to the higher absorption coefficient from incident solar radiation and a high melting point [27]. Titanium (Ti) is utilized in alloy form for parts in high-speed aircraft because it is a lightweight, high-strength, low-corrosion structural metal. It can be directly combined with a variety of nonmetals, such as hydrogen, halogen, nitrogen, carbon, boron, silicon, and sulfur, to form new compounds such as titanium nitride (TiN), titanium carbide (TiC), and titanium borides (TiB and TiB_2). These new compounds are extremely stable, hard, and refractory at high temperatures [28]. The design process of the developed infinity-shaped solar energy absorber is discussed in Section 2, and the results, with in-depth discussion, are provided in Section 3; the paper ends with the concluding notes presented in Section 4.

2. Design and Modeling

Figure 1 depicts the structure of the solar absorber with an infinity pattern. In that design, a substrate is made of gallium arsenide (GaAs) and a resonator with an infinity shape is constructed with titanium (Ti) material positioned above the GaAs layer. Figure 1a shows a 3D version of a broadband absorber with an infinite shape. Figure 1b, c shows the top and front views of a broadband solar energy absorber, respectively. The parameters of the developed broadband design are: structural length L is 600 nm; substrate gallium arsenide (GaAs) thickness K_s is 600 nm; titanium infinity-shaped resonator thickness K_r is 500 nm, as exhibited in Figure 1c. The infinity shape's width and length are T_w = 200 nm and T_l = 500 nm, respectively, as showcased in Figure 1c. COMSOL Multiphysics and the finite element method (FEM) are used to numerically calculate the design using planar light, with wavelengths between 0.2 and 3 μm in the *z*-axis path. Both the *x*- and *y*-axis directions use the periodic boundary conditions. Gallium arsenide (GaAs) has a refractive index of 3.7851 [7]. The refractive index data of titanium (Ti) and gallium arsenide (GaAs) have been taken from CRC Press.

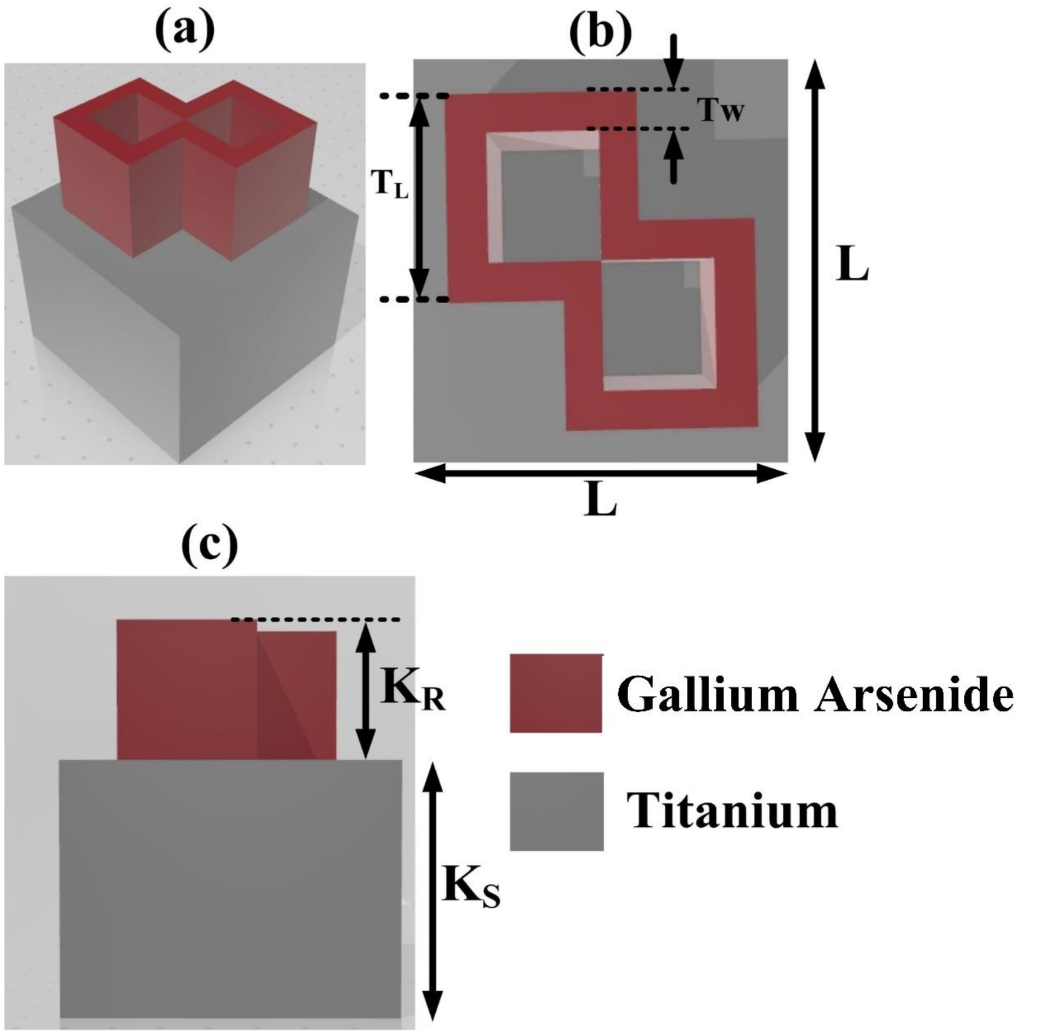

Figure 1. Structure of the infinity-shaped broadband solar absorber. (**a**) Absorber structure in 3D view; (**b**) broadband solar absorber structure, top view; (**c**) broadband solar absorber structure, front view; the parameters: structural length L is 600 nm, substrate gallium arsenide (GaAs) thickness K_s is 900 nm, infinity-shaped titanium resonator thickness K_r is 500 nm. Width T_w and length T_l, of the infinity shapes are 500 and 200 nm, respectively. The broadband figure is not the same as the developed scale.

3. Results and Discussion

In this section, the analysis of the proposed infinity-shaped broadband solar absorber is presented. First, the absorption analysis to demonstrate the high and broadband absorption achieved by the proposed absorber is provided, followed by the electric field intensity response of the proposed absorber at various wavelengths to confirm the achieved results. Later in this section, a procedure to attain the optimal structure is discussed in detail by varying different characteristics. At last, the desired characteristics in an ideal solar absorber are investigated for the proposed structure, and how to achieve angle- as well as polarization-independent absorption is discussed in detail. The section ends by comparing the proposed structure with available designs to demonstrate the remarkable performance of the proposed design.

3.1. Absorption Analysis

The absorption, reflectance, and transmittance of the infinity-shaped broadband absorber presented in Figure 1 are investigated, as shown in Figure 2. In Figure 2a, the letters R and T stand for the reflectance and transmittance characteristics. According to the formula A = 1 – R – T, the presented broadband solar absorber design, using a resonator metamaterial with a Ti metal pattern, matches impedance and minimizes light reflection [29]. For the 0.2 to 3 μm range in the ultraviolet (UV) region to the mid-infrared region (MIR) with a bandwidth of 2800 nm, an absorption rate above 90% is observed. For the wide bandwidth of 2800 nm, the absorption rate of the infinity-shaped broadband solar absorber is observed at 93.93%. Moreover, for the bandwidth of 350 nm, the proposed infinity-shaped broadband solar absorber achieved more than a 95% absorption rate from 0.2 to 0.55 μm. The proposed broadband absorber's average absorption rate for the previously indicated bandwidth range is 96.99%. Additionally, for a bandwidth of 760 nm, the average absorption rate is 95.90% for the wavelength range of 2.24 to 3 μm. We can also examine the six peaks, which correspond to the highest absorption values at 0.4, 0.55, 1.65, 2.24, 2.6, and 3 μm, with absorptance rates of 99.19%, 95.94%, 99.2%, 95.44%, 95.73%, and 97.64%. The suggested broadband solar absorber has average absorption rates of 97.11%, 94.45%, 92.85%, and 96.53%, respectively, in the areas of ultraviolet to the MIR. The excellent average absorption for the overall ranges of 0.2 to 3 μm of the broadband solar absorber is 93.93%. The scope of this manuscript is to theoretically demonstrate and numerically investigate the concept of infinity-shaped solar absorbers for achieving broadband- and polarization-independent absorption. Note that in all our simulations and analysis, we have assumed practical parameters for the presented design, although previous research has shown almost identical experimental and numerical absorption plots [30]. To determine the incident sun energy of the global band, we have utilized an Air Mass Index of 1.5 (AM 1.5) [31].

$$\eta_A = \frac{\int_{\lambda_{min}}^{\lambda_{max}} (1 - R(\omega)).I_{AM1.5}(\omega).d\omega}{\int_{\lambda_{min}}^{\lambda_{max}} I_{AM1.5}(\omega).d\omega} \quad (1)$$

According to the equation above, broadband solar absorption under normal conditions is denoted by A, the broadband irradiance is denoted by $I_{AM1.5}$ for an air mass of 1.5, and the reflectance is denoted by R.

The proposed broadband solar absorber's absorptance response with respect to the $AM1.5$ radiation and total missed energy is demonstrated in Figure 2b. The sky blue region displays the $AM1.5$ spectrum curve, and the grey region displays the proposed broadband solar absorber efficiency under solar radiation. These values were calculated using the numerator of Equation (1), and missed energy absorption was assessed from the denominator [32]. The proposed infinity-shaped broadband solar energy absorber is greatly focused in the ultraviolet to MIR band of solar light. To get a greater capacity of broadband solar absorption, the absorption rate needs to be higher; hence, the missed energy quantity is nearly zero in the MIR region from the ultraviolet region [33].

3.2. Analysis of Electric Field Intensity to Validate Broadband Absorption of Proposed Infinity-Shaped Solar Absorber

Analysis of the electric field intensity amount for the developed infinity-shaped broadband absorber is expressed for the six absorptance peaks as λ_1, λ_2, λ_3, λ_4, λ_5, and λ_6, correspondingly, to examine the physical characteristics of broadband absorber absorption.

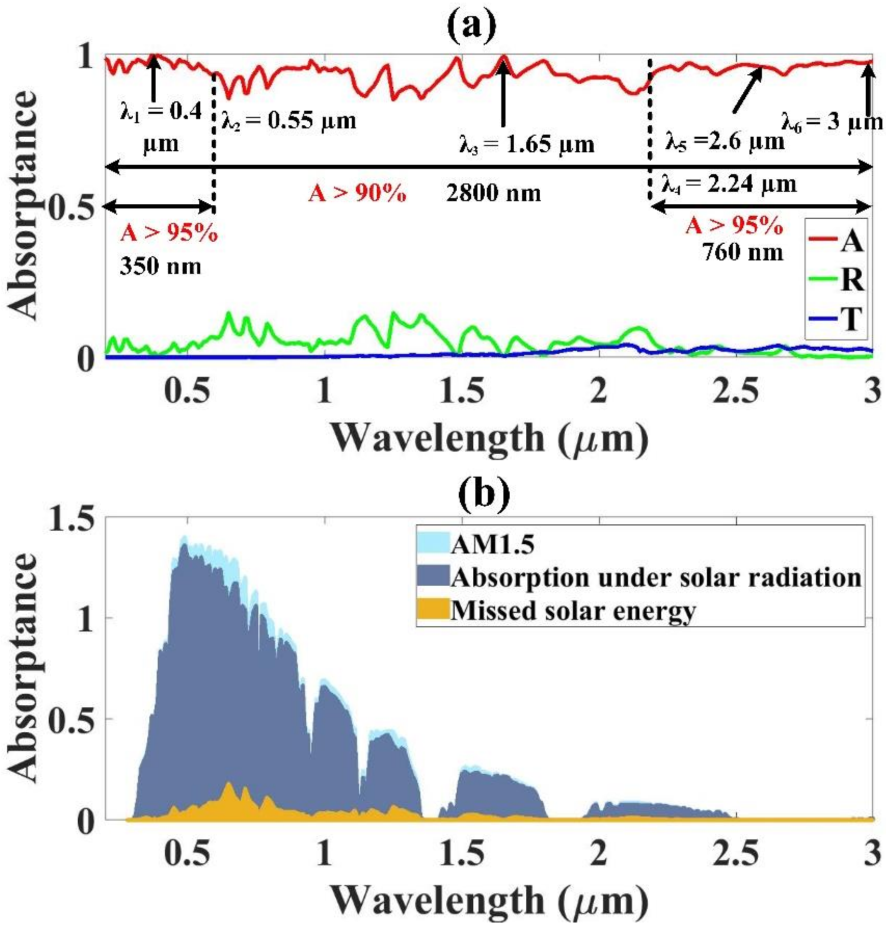

Figure 2. (**a**) The infinity-shaped broadband solar absorber's ultra-wideband absorption for wavelengths between 0.2 and 3 μm, and (**b**) the absorptance of the infinity-shaped broadband solar absorber for the *AM*1.5 broadband spectrum and the total missed energy. The figure demonstrates the higher performance of the proposed infinity-shaped solar absorber for the whole solar spectrum, from the UV to MIR areas, and the *AM*1.5 plot indicates the high absorption under solar radiation and the small quantity of missing energy across the UV to visible areas.

The x–y plane electric field intensity is shown in Figure 3a–f, and the x–z plane electric field intensity is shown in Figure 3g–l. A wavelength of λ_1 = 0.4 μm is regarded as the topmost absorption rate of the developed broadband absorber structure, and we note the average absorption rate of 99.91% at this wavelength. In Figure 3a, the GaAs substrate is subjected to the greatest electric field. Thereafter, Figure 3g describes the quantity of scattered electric fields at the upper substrate level portion. At the wavelength of λ_2 = 0.55 μm, the absorption rate is 95.94%. On the other hand, the electric field is not dispersed quite as high compared to the first peak on the substrate surface, as depicted in Figure 3b. The difference between these two layers is the electric field quantity, which is a little dispersed in the lower region of the broadband absorber, as demonstrated in Figure 3h. The third highest absorption rate is 99.2% at wavelength λ_3 = 1.65 μm. Then, Figure 3c reports on the infinity-shaped broadband solar titanium resonator, and the electric field intensity is more concentrated than before. In Figure 3i, a higher portion of the substrate layer is covered with a more evenly distributed layer than the second peak in terms of the quantity of electric field strength of the broadband solar absorber. The wavelength of λ_4 = 2.24 μm is observed as the fourth-highest absorption rate of 95.44%. Figure 3d shows the high electric field intensity of broadband solar infinity-shaped absorber inner edges compared to the third peak mentioned above. Figure 3j compares the broadband electric field intensity of the third peak of the broadband solar absorber, and the results reveal that the electric field intensity is very high and is spread throughout the substrate layer of the broadband solar absorber. The fifth absorption point is almost 95.73% at wavelength λ_5 = 2.6 µm. In Figure 3e, the titanium resonator and the gallium arsenide layer both have a similar distribution of electric field intensity compared to the previous case.

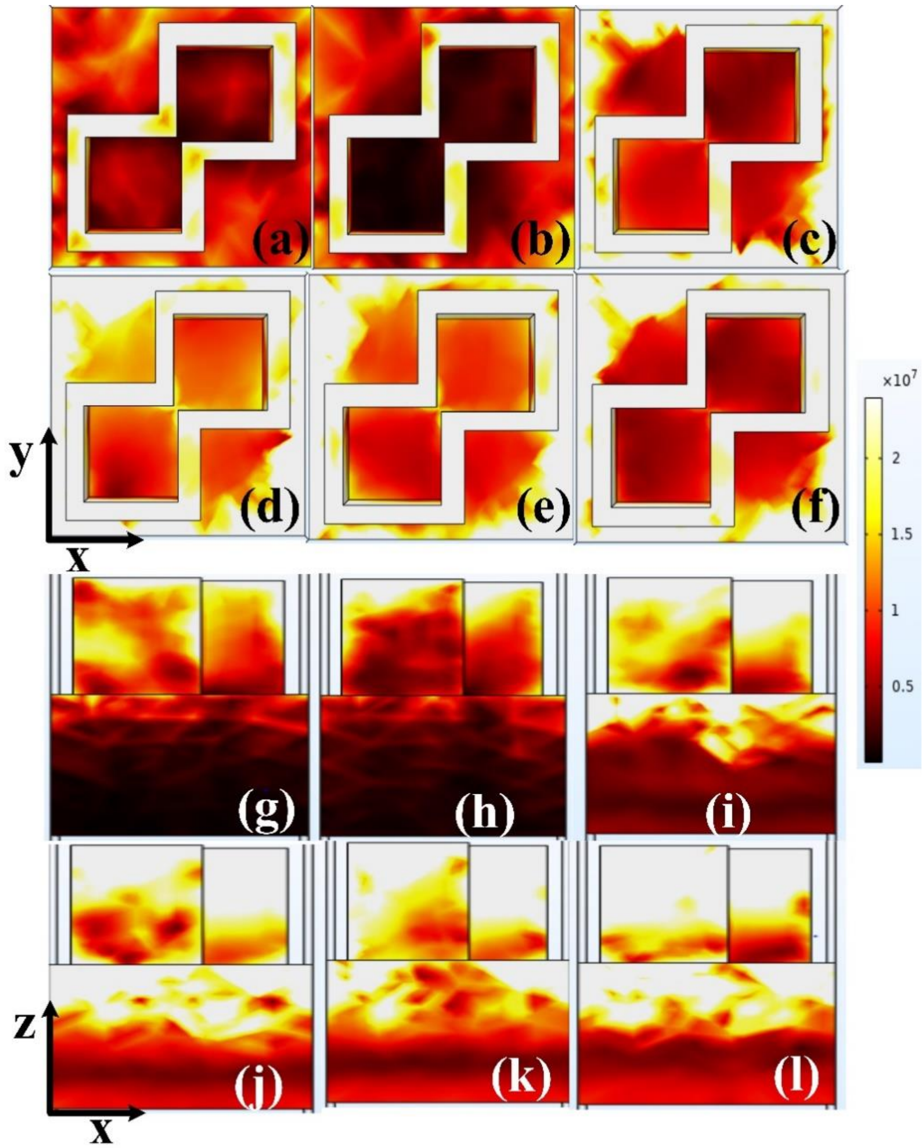

Figure 3. Broadband electric field strength in the x–y plane at wavelengths (**a**) λ_1 = 0.4, (**b**) λ_2 = 0.55, (**c**) λ_3 = 1.65, (**d**) λ_4 = 2.24, (**e**) λ_5 = 2.6, and (**f**) λ_6 = 3 µm, and wavelengths in the x–z plane (**g**) λ_1 = 0.4, (**h**) λ_2 = 0.55, (**i**) λ_3 = 1.65, (**j**) λ_4 = 2.24, (**k**) λ_5 = 2.6, and (**l**) λ_6 = 3 µm. The electric field intensity plots confirm the high absorption and broadband response of the proposed infinity-shaped solar absorber by demonstrating the high number of electric fields concentrated at the resonator level and some portions of the substrate while the rest of the substrate contributes by reflecting the solar energy to be absorbed by the resonator.

Figure 3k shows that the visibility of electric field intensity in some volumes is dispersed at the identical part of the broadband solar absorber substrate level if we consider the previous case. The wavelength of λ_6 = 3 µm is the sixth-highest absorption rate of the broadband solar absorber, with an absorption of 97.64%. Figure 3f showcases the inner and outer parts of an infinity-shaped broadband solar absorber's electric field intensity. In Figure 3l, the significant electric field intensity is distributed at a larger part of the resonator and a smaller part of the substrate layer of the absorber.

To attain an optimal structure, we continued our analysis on the average absorptance rate of the infinity-shaped broadband solar absorber by changing the numerous structural parameters, such as the length, width, and thickness of the infinity-shaped broadband solar absorber-based resonator; the GaAs thickness results are mentioned in Figure 4. The increased thickness of the infinity form resonator, from 500 to 1000 nm, with a difference of 100 nm, is given in Figure 4a for the wavelength range of 0.2 to 3 μm. The increase in the thickness of the resonator reveals that the absorption rate is 99.19% to 97.23% at the wavelength of λ1. When we changed the thickness, the average absorption rate decreased at the fourth wavelength of λ_4, from 95.44% to 95.32%. The same situation can also be reported for the rest of the wavelengths, e.g., λ_2, λ_3, λ_5, and λ_6 show a decreased absorptance rate from 95.94%, 99.2%, 95.73%, and 97.64% to 95.08%, 97.27%, 95.32%, and 95.89%, respectively. When we increased the resonator thickness, the overall average broadband absorption rates decreased from 97.64% to 95.89%. For a resonator thickness of 500 nm, the maximum absorption was noted to be above 90%, and the average absorption at this particular resonator thickness in all four regions was also higher than 90%; hence, the resonator thickness was kept at 500 nm. In Figure 4b, the same effect of the absorption response is shown by a fermi plot. From this figure, it is noticed that in the ultraviolet region, when we increase the broadband solar absorber resonator thickness from 500 to 1000 nm, the average absorption response is reduced.

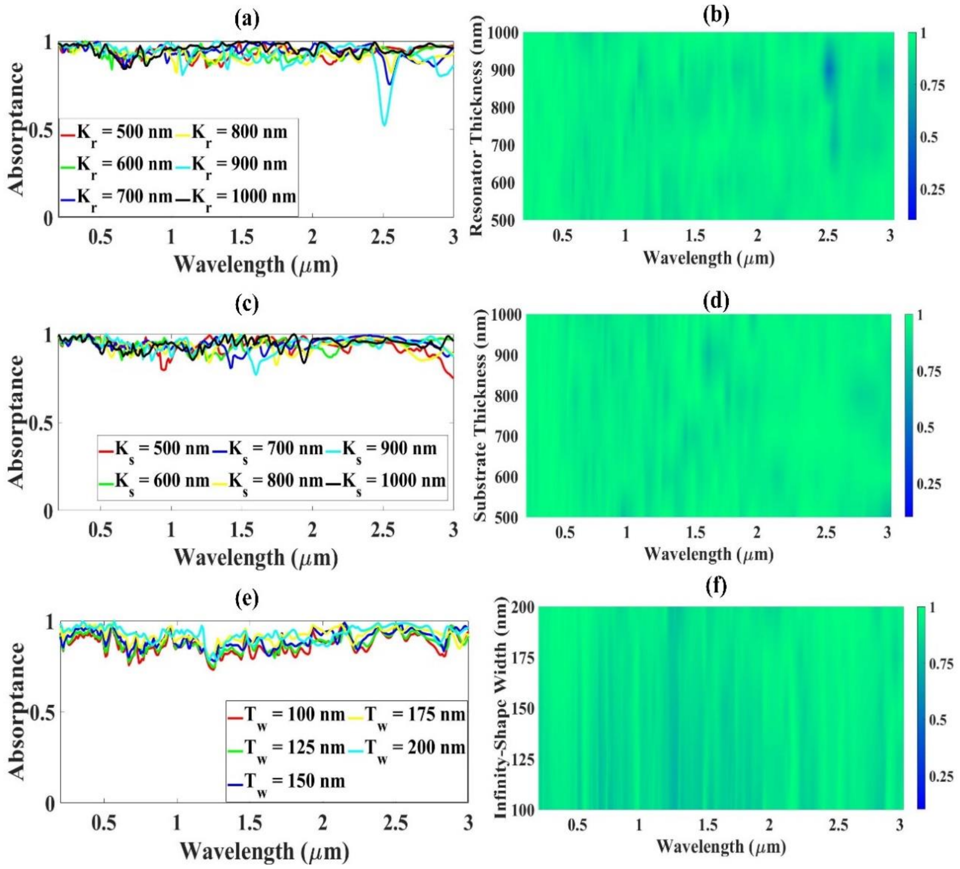

Figure 4. The proposed infinity-shaped broadband absorber's absorption rate: (**a**) output of increasing the broadband solar absorber's structural length and respective width, L; (**b**) output of the broadband solar absorber's structural length and respective width, L, demonstrated by color plot effect; (**c**) GaAs broadband material thickness, K_s, increasing on the broadband spectrum; (**d**) GaAs broadband material thickness, K_s, increasing on the broadband spectrum, demonstrated by fermi plot; (**e**) the output of increasing the infinity-shaped broadband solar absorber's material width, T_w, (**f**) demonstration of the increased infinity-shaped broadband solar absorber's material width, T_w, by color plot.

3.3. Parametric Optimization to Obtain Optimal Structure

Additionally, we analyzed the variations in the proposed infinity-shaped solar energy absorber's substrate thickness. When the broadband substrate depth is raised from 500 to 1000 nm, with a difference of 100 nm, the corresponding outputs are shown in Figure 4c. Hence, when we gradually increase the substrate depth, the absorption rate at wavelength λ_1 is decreased from 99.22% to 98.27%. The same situation for the second absorptance peak λ_2 is observed, in that the absorption decreases from 97.01% to 95.62%. Absorptance peaks such as λ_2, λ_3, λ_4, and λ_5 follow the same phenomenon. In Figure 4d, the substrate depth affecting the absorption rate is shown by a fermi plot. From this figure, it can be noticed that in the ultraviolet region, the absorption rate is reduced when the broadband solar absorber's substrate depth increases between 500 and 1000 nm. Consequently, the average absorption of the proposed infinity-shaped solar energy absorber is nearly the same in the ultraviolet area, while it decreases in the violet region. Moreover, in the regions of NIR and MIR, the average absorption rate of infinity-shaped resonator thickness is also decreased.

To show various observations, we varied the infinity shape width from 100 to 200 nm with a difference of 25 nm. The observed parameter and corresponding line plots and fermi plots are shown in Figure 4e. When we increase the infinity-shaped resonator width from 100 to 200 nm, the average absorption rate increases from 93.97% to 96.17%. Resonator width can widely affect the ultraviolet region between the range 100 to 200 nm, and average absorption increases from 90.05% to 96.55%, as shown in Figure 4f.

3.4. Angle- and Polarization-Insensitiveness Investigation

We now discuss how polarization affects a proposed absorber structure in both the transverse electric (TE) and transverse magnetic (TM) modes, as demonstrated in Figure 5. First, we noted the variation of incidence angles on the infinity-shaped broadband solar absorber between 0 and 80 degrees by a difference in 10 degrees at the wavelength parameter of 0.2–3 μm; Figure 5a,b show the appropriate fermi plot, respectively. The transverse electric (TE) mode is mentioned in Figure 5a. With the same situation at the absorptance peaks of λ_1, λ_2, λ_3, λ_5 and λ_6, the absorptance response decreases from 99.19%, 95.94%, 99.2%, 95.44%, 95.73%, and 97.27% to 40.93%, 18.66%, 63.3%, 51.34%, 51.45%, and 58.93%, respectively. In Figure 5b, the variation of the angle of incidence (degree) in the TE mode is shown by a fermi plot. It can be stated that absorption between 0° to 50° does not change, and so it is a wide-angle-insensitive region. From 50° to 70°, the UV and vis regions show an average absorption rate of below 90%, and the NIR and MIR showcase an absorption level of above 95%.

The infinity-shaped broadband solar absorber is in the range between 0 and 80 degrees, by a difference of 10 degrees, at the wavelength parameter of 0.2–3 μm, and Figure 5c,d illustrate the matching fermi plot, respectively. The same situation is observed for TE mode for the absorptance peaks of λ_1, λ_2, λ_3, λ_5, and λ_6; the absorptance response decreases from 99.19%, 95.95%, 99.63%, 96.77%, 98.37%, and 98.91%, to 40.93%, 18.66%, 63.11%, 50.31%, 54.71%, and 58.67%, respectively. Hence, the variation in TM mode is almost the same as the variation in TE mode mentioned before. In Figure 5d, the variation of the angle of incidence (degree) in TM mode is shown in the fermi plot. Hence, it can be reported that for the TM mode, absorption between 0° to 50° has not changed, and so, it is a wide angle-insensitive region. The ultraviolet and visible areas have been shown to have an average absorption rate of below 90% from 50 to 70 degrees; it shifts from 66.67% to 43.65% in the UV region and in the vis region from 69.37% to 31.42%. Otherwise, in the NIR and MIR, it is above 95%. From the ultraviolet to NIR, we can observe an average broadband absorption rate of above 95% with 1100 nm bandwidth, and moreover, we also note good absorption for the 2800 nm bandwidth; the change in polarization does not affect it, and for 0° to 50°, we achieved the large angular absorption response, as demonstrated in Table 1, which demonstrates the higher performance of the proposed infinity-shaped solar energy absorber in the available literature. Therefore, the developed infinity-shaped broadband solar absorber can be used in many solar systems (photovoltaics, generators, and heat transfer) [34] because of its broadband, efficiency, and abovementioned characteristics.

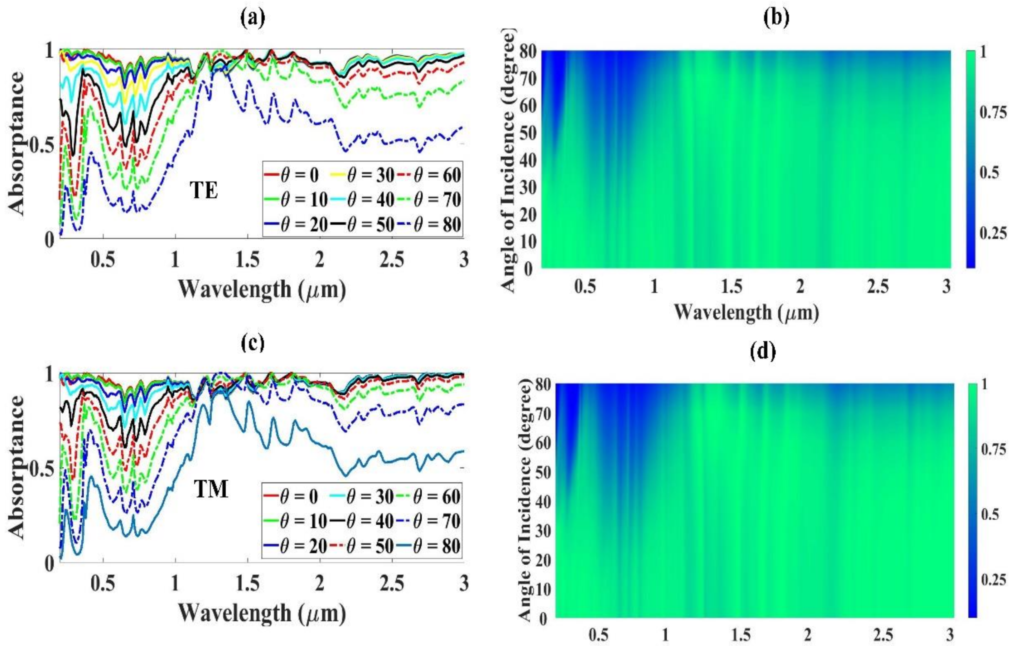

Figure 5. Absorption rates of the infinity-shaped broadband solar absorber: (**a**) for TE mode from 0 to 80 degrees, exhibiting identical absorption in NIR and MIR; (**b**) displaying the change in absorption, with a color plot for the UV and vis regions; (**c**) for TM mode from 0 to 80 degrees, exhibiting identical absorption in NIR and MIR; (**d**) displaying the change in absorption with a color plot for the UV and vis regions. For both TE and TM modes, the absorption responses for all angles are identical, depicting polarization-independent characteristics.

Table 1. Difference between the developed infinity-shaped broadband absorber and the available literature.

Ref	Overall Mean Absorption	Bandwidth (Absorption > 90%)	Bandwidth (Absorption > 95%)	Angle-Insensitive	Polarization-Insensitive
Ref. [33]	More than 90%	1110	-	0° to 40°	Yes
Ref. [35]	More than 90%	1007	-	0° to 45°	-
Ref. [36]	93.17%	1759	-	0° to 45°	Yes
Ref. [37]	93.26	1650	-	0° to 70°	Yes
Ref. [38]	More than 90%	1310	-	0° to 60°	Yes
Ref. [39]	More than 90%	1000	-	-	Yes
Ref. [40]	More than 90%	1264	-	0° to 45°	-
Proposed Study	93.93%	2800 nm	1110 nm	0° to 50°	Yes

4. Conclusions

In this paper, we have examined an infinity-shaped broadband solar energy absorber simulated by COMSOL Multiphysics and the FEM technique. The solar energy absorber structure presented here is developed for electromagnetic wave absorption for the various wavelengths between 0.2 and 3 μm. The developed absorber demonstrates a broadband absorption rate above 90% for the 2800 nm bandwidth from 0.2 to 3 μm, and the average absorption rate is 93.93%. Moreover, the average solar absorption rate for the 1110 nm band from 0.2 to 0.55 μm and 2.24 to 3 μm is 96.25%, and an absorption rate above 95% is also observed for this band. Additionally, at the absorptance peaks such as 0.4, 0.55, 1.65, 2.24, 2.6, and 3 μm, the developed structure can absorb solar energy at 99.19%, 95.94%, 99.2%, 95.44%, 95.73%, and 97.64%, respectively. For these six peaks, the electric field intensity has been determined and discovered. Additionally, calculations have been made to determine how developed broadband structural characteristics such as resonator and substrate thickness affect solar energy absorption. Then, we explored the polarization by changing modes, and the angular results from 0° to 80° validated the large angular- and polarization-independent response of the proposed structure.

Author Contributions: Conceptualization, S.K.P. and M.A.; methodology, M.A., B.B.H., S.K.P. and J.S.; software, B.B.H., J.S. and M.A.; validation, B.B.H., K.A. and A.A.; formal analysis, S.K.P. and J.S.; investigation, K.A. and J.S.; resources, A.A. and B.B.H.; writing—original draft preparation, all authors; writing—review and editing, M.A. and S.K.P.; supervision, S.K.P. and M.A. All authors have read and agreed to the published version of the manuscript.

Funding: This research was funded by Deputyship for Research and Innovation, Ministry of Education, Saudi Arabia grant number 223202.

Institutional Review Board Statement: Not Applicable.

Informed Consent Statement: Not Applicable.

Data Availability Statement: The data will be made available upon reasonable request to the corresponding author.

Acknowledgments: The authors extend their appreciation to the Deputyship for Research & Innovation, Ministry of Education, Saudi Arabia, for funding this research work.

Conflicts of Interest: The authors declare no conflict of interest.

References

1. Kekecs, Z.; Nagy, T.; Varga, K. The effectiveness of suggestive techniques in reducing postoperative side effects: A meta-analysis of randomized controlled trials. *Anesth. Analg.* **2014**, *119*, 1407–1419. [CrossRef] [PubMed]
2. Ganose, A.M.; Matsumoto, S.; Buckeridge, J.; Scanlon, D.O. Defect Engineering of Earth-Abundant Solar Absorbers BiSI and BiSeI. *Chem. Mater.* **2018**, *30*, 3827–3835. [CrossRef] [PubMed]
3. Denchak, M. *Fossil Fuels: The Dirty Facts*; NRDC, Natural Resources Defense Council: New York, NY, USA, 2018; pp. 1–26.
4. Fócil, E.; Zavala, M. Funcionalidad para actividades de la vida diaria en adultos mayores rurales de Cárdenas, Tabasco, México Functionality for daily living activities in rural elderly from Cardenas. *RFS Rev. Fac. Salud* **2015**, *6*, 12–19. [CrossRef]
5. Yang, L.; Chen, G.; Zhang, N.; Xu, Y.; Xu, X. Sustainable Biochar-Based Solar Absorbers for High-Performance Solar-Driven Steam Generation and Water Purification. *ACS Sustain. Chem. Eng.* **2019**, *7*, 19311–19320. [CrossRef]
6. Krumme, J.-P.; Hack, R.A.A.; Raaijmakers, I.J.M.M.; Cazzaniga, A.; Crovetto, A.; Ettlinger, R.B.; Canulescu, S.; Hansen, O.; Pryds, N.; Schou, J.J.; et al. Photovoltaic Energy Conversion, 2003. Proceedings of 3rd World Conference on. *Thin Solid Films* **2011**, *3*, 1–4.
7. Sayre, L.; Camarillo Abad, E.; Pearce, P.; Chausse, P.; Coulon, P.M.; Shields, P.; Johnson, A.; Hirst, L.C. Ultra-thin GaAs solar cells with nanophotonic metal-dielectric diffraction gratings fabricated with displacement Talbot lithography. *Prog. Photovoltaics Res. Appl.* **2022**, *30*, 96–108. [CrossRef]
8. Gong, J.; Liang, J.; Sumathy, K. Review on dye-sensitized solar cells (DSSCs): Fundamental concepts and novel materials. *Renew. Sustain. Energy Rev.* **2012**, *16*, 5848–5860. [CrossRef]
9. Zhao, X.G.; Yang, D.; Sun, Y.; Li, T.; Zhang, L.; Yu, L.; Zunger, A. Cu-In Halide Perovskite Solar Absorbers. *J. Am. Chem. Soc.* **2017**, *139*, 6718–6725. [CrossRef]
10. Patel, S.K.; Surve, J.; Parmar, J.; Katkar, V.; Jadeja, R.; Taya, S.A.; Ahmed, K. Graphene-based metasurface solar absorber design for the visible and near-infrared region with behavior prediction using Polynomial Regression. *Optik* **2022**, *262*, 169298. [CrossRef]
11. Patel, S.K.; Surve, J.; Prajapati, P.; Taya, S.A. Design of an ultra-wideband solar energy absorber with wide-angle and polarization independent characteristics. *Opt. Mater.* **2022**, *131*, 112683. [CrossRef]
12. Ding, F.; Cui, Y.; Ge, X.; Jin, Y.; He, S. Ultra-broadband microwave metamaterial absorber. *Appl. Phys. Lett.* **2012**, *100*, 103506. [CrossRef]
13. Wang, H.; Wang, L. Perfect selective metamaterial solar absorbers. *Opt. Express* **2013**, *21*, A1078. [CrossRef] [PubMed]
14. Gomez-Garcia, F.; Gonzalez-Aguilar, J.; Tamayo-Pacheco, S.; Olalde, G.; Romero, M. Numerical analysis of radiation propagation in a multi-layer volumetric solar absorber composed of a stack of square grids. *Sol. Energy* **2015**, *121*, 94–102. [CrossRef]
15. Abdulkarim, Y.I.; Özkan Alkurt, F.; Awl, H.N.; Altıntaş, O.; Muhammadsharif, F.F.; Appasani, B.; Bakır, M.; Karaaslan, M.; Taouzari, M.; Dong, J. A Symmetrical Terahertz Triple-Band Metamaterial Absorber Using a Four-Capacitance Loaded Complementary Circular Split Ring Resonator and an Ultra-Thin ZnSe Substrate. *Symmetry* **2022**, *14*, 1477. [CrossRef]
16. Banerjee, S.; Dutta, P.; Basu, S.; Mishra, S.K.; Appasani, B.; Nanda, S.; Abdulkarim, Y.I.; Muhammadsharif, F.F.; Dong, J.; Jha, A.V.; et al. A New Design of a Terahertz Metamaterial Absorber for Gas Sensing Applications. *Symmetry* **2022**, *15*, 24. [CrossRef]

17. Lai, S.; Liu, G.; Guo, Y.; Liu, Y. Design of an Optically Transparent Microwave Absorber Based on Coding Metasurface. *Symmetry* **2022**, *14*, 2217. [CrossRef]
18. Mittal, M.K.; Varun; Saini, R.P.; Singal, S.K. Effective efficiency of solar air heaters having different types of roughness elements on the absorber plate. *Energy* **2007**, *32*, 739–745. [CrossRef]
19. Romanyuk, Y.E.; Fella, C.M.; Uhl, A.R.; Werner, M.; Tiwari, A.N.; Schnabel, T.; Ahlswede, E. Recent trends in direct solution coating of kesterite absorber layers in solar cells. *Sol. Energy Mater. Sol. Cells* **2013**, *119*, 181–189. [CrossRef]
20. Ahmad, F.; Lakhtakia, A.; Monk, P.B. Double-absorber thin-film solar cell with 34% efficiency. *Appl. Phys. Lett.* **2020**, *117*, 033901. [CrossRef]
21. Li, S.Y.; Hägglund, C.; Ren, Y.; Scragg, J.J.S.; Larsen, J.K.; Frisk, C.; Rudisch, K.; Englund, S.; Platzer-Björkman, C. Optical properties of reactively sputtered Cu2ZnSnS4 solar absorbers determined by spectroscopic ellipsometry and spectrophotometry. *Sol. Energy Mater. Sol. Cells* **2016**, *149*, 170–178. [CrossRef]
22. Zheng, Y.; Wu, P.; Yang, H.; Yi, Z.; Luo, Y.; Liu, L.; Song, Q.; Pan, M.; Zhang, J.; Cai, P. High efficiency Titanium oxides and nitrides ultra-broadband solar energy absorber and thermal emitter from 200 nm to 2600 nm. *Opt. Laser Technol.* **2022**, *150*, 108002. [CrossRef]
23. Zhou, Y.; Chen, J.; Bakr, O.M.; Mohammed, O.F. Metal Halide Perovskites for X-ray Imaging Scintillators and Detectors. *ACS Energy Lett.* **2021**, *6*, 739–768. [CrossRef]
24. Fan, P.; Wu, H.; Zhong, M.; Zhang, H.; Bai, B.; Jin, G. Large-scale cauliflower-shaped hierarchical copper nanostructures for efficient photothermal conversion. *Nanoscale* **2016**, *8*, 14617–14624. [CrossRef] [PubMed]
25. Zhou, Z.; Chen, Y.; Tian, Y.; Liang, J.; Yang, W. Ultra-broadband metamaterial perfect solar absorber with polarization-independent and large incident angle-insensitive. *Opt. Laser Technol.* **2022**, *156*, 108591. [CrossRef]
26. Jiang, J.; Xu, Y.; Li, Y.; Ren, L.; Chen, F.; Cheng, S.; Yang, W.; Ma, C.; Wang, Z.; Zhou, X. Ultra-broadband, near-perfect and thin-film scale solar absorber based on semiconductor-metal nanocone. *Optik* **2021**, *246*, 167855. [CrossRef]
27. Sani, E.; Meucci, M.; Mercatelli, L.; Balbo, A.; Musa, C.; Licheri, R.; Orrù, R.; Cao, G. Titanium diboride ceramics for solar thermal absorbers. *Sol. Energy Mater. Sol. Cells* **2017**, *169*, 313–319. [CrossRef]
28. Ignatiev, A.; O'Neill, P.; Zajac, G. The surface microstructure optical properties relationship in solar absorbers: Black chrome. *Sol. Energy Mater.* **1979**, *1*, 69–79. [CrossRef]
29. Rufangura, P.; Sabah, C. Design and characterization of a dual-band perfect metamaterial absorber for solar cell applications. *J. Alloys Compd.* **2016**, *671*, 43–50. [CrossRef]
30. NREL. Reference Air Mass 1.5 Spectra. *Grid Mod.* **2019**, 4.
31. Azad, A.K.; Kort-Kamp, W.J.M.; Sykora, M.; Weisse-Bernstein, N.R.; Luk, T.S.; Taylor, A.J.; Dalvit, D.A.R.; Chen, H.T. Metasurface Broadband Solar Absorber. *Sci. Rep.* **2016**, *6*, 20347. [CrossRef]
32. Mazzio, K.A.; Luscombe, C.K. The future of organic photovoltaics. *Chem. Soc. Rev.* **2015**, *44*, 78–90. [CrossRef] [PubMed]
33. Liu, Z.; Liu, G.; Huang, Z.; Liu, X.; Fu, G. Ultra-broadband perfect solar absorber by an ultra-thin refractory titanium nitride meta-surface. *Sol. Energy Mater. Sol. Cells* **2018**, *179*, 346–352. [CrossRef]
34. Jia, X.; Yin, S.; Tang, Z. A Simple Metamaterial for High-Performance Spectrum-Selective Absorption in the Visible Region. *Symmetry* **2022**, *14*, 2402. [CrossRef]
35. Liu, Z.; Liu, G.; Liu, X.; Wang, Y.; Fu, G. Titanium resonators based ultra-broadband perfect light absorber. *Opt. Mater.* **2018**, *83*, 118–123. [CrossRef]
36. Yu, P.; Yang, H.; Chen, X.; Yi, Z.; Yao, W.; Chen, J.; Yi, Y.; Wu, P. Ultra-wideband solar absorber based on refractory titanium metal. *Renew. Energy* **2020**, *158*, 227–235. [CrossRef]
37. Gao, H.; Peng, W.; Chu, S.; Cui, W.; Liu, Z.; Yu, L.; Jing, Z. Refractory ultra-broadband perfect absorber from visible to near-infrared. *Nanomaterials* **2018**, *8*, 1038. [CrossRef] [PubMed]
38. Soydan, M.C.; Ghobadi, A.; Yildirim, D.U.; Erturk, V.B.; Ozbay, E. All Ceramic-Based Metal-Free Ultra-broadband Perfect Absorber. *Plasmonics* **2019**, *14*, 1801–1815. [CrossRef]
39. Tian, X.; Li, Z.-Y. Visible-near infrared ultra-broadband polarization-independent metamaterial perfect absorber involving phase-change materials. *Photonics Res.* **2016**, *4*, 146. [CrossRef]
40. Yu, P.; Chen, X.; Yi, Z.; Tang, Y.; Yang, H.; Zhou, Z.; Duan, T.; Cheng, S.; Zhang, J.; Yi, Y. A numerical research of wideband solar absorber based on refractory metal from visible to near infrared. *Opt. Mater.* **2019**, *97*, 109400. [CrossRef]